Negative P-T slopes characterize phase change processes: Case of the Ge_{1}Sb_{2}Te_{4} phase change alloy

B. Kalkan, S. Sen, B. G. Aitken, S. V. Raju, and S. M. Clark

Phys. Rev. B **84**, 014202 — Published 29 July 2011

DOI: 10.1103/PhysRevB.84.014202

Negative P-T slopes characterize phase change processes: the case for the $Ge_1Sb_2Te_4$ phase change alloy

B. Kalkan, [1] S. Sen, [2] B.G. Aitken[3] S.V. Raju[1] and S. M. Clark[1,4]

[1] Advanced Light Source, Lawrence Berkeley Laboratory, Berkeley, California 20015, USA

[2]Department of Chemical Engineering and Materials Science, University of California,, Davis, California 95616, USA

[3]Glass Research Division, SP-FR-05, Corning Incorporated, Corning, NY 14831, USA

[4]Department of Earth and Planetary Sciences, University of California, Berkeley, California 94720, USA

The crystalline, liquid and amorphous phase stabilities and transformations of the $Ge_1Sb_2Te_4$ (GST124) alloy are investigated as a function of pressure and temperature using synchrotron diffraction experiments in a diamond anvil cell. The results indicate that the solid-state amorphization of the cubic GST124 phase under high pressure may correspond to a metastable extension of the stability field of the GST124 liquid along a hexagonal crystal-liquid phase boundary with a negative P-T slope. The internal pressures generated during phase change are shown to be too small to affect phase stability. However, they may be important in understanding reliability issues related to thermomechanical stress development in phase change random access memory structures.

PACS numbers: 61.50.Ks, 64.70.kd, 62.50.-p, 64.60.cn, 81.30.Hd

I. Introduction

Phase-change alloys in the Ge-Sb-Te system along the $GeTe$-Sb_2Te_3 tie line show rapid thermal or electrical switching between crystalline and glassy/amorphous phases under suitable conditions and are of extraordinary technological importance in rewritable optical and electronic memory applications [e.g. in digital video disks (DVD)] [1-3]. The concept of rewritable data storage in phase-change materials involves recording the data using a intense nanosecond laser or voltage pulse that melts the crystal phase locally (over a few hundred μm) and the melt subsequently quenches into amorphous phase. The unusually large difference in optical absorption and reflectivity (for optical storage) or in the electrical resistivity (for electronic storage) between the crystalline and amorphous phases allows the reading of the data using a low-intensity laser beam (for optical storage). Subsequently, a laser pulse of intermediate power is used to heat the amorphous phase above its crystallization temperature to recrystallize and erase the data [1].

The stable crystal structure of Ge-Sb-Te alloys along the $GeTe$-Sb_2Te_3 tie line under ambient conditions is hexagonal [4]. However, amorphous GST (*a*-GST) thin films crystallize upon laser irradiation into *c*-GST, a metastable, face-centered cubic (fcc) rocksalt structure with Te atoms occupying one fcc sublattice while Ge/Sb atoms randomly occupy the other [1]. This rocksalt structure is relevant for the phase-change applications and is also formed first upon thermal heating of the amorphous material to ~ 393 K. Further heating to higher temperatures of ~ 453 K eventually transforms the rocksalt structure into the stable hexagonal structure [5-7]. It is to be noted that the crystal structure of the *c*-GST phase is characterized by the presence of a large number of vacancies in the Ge/Sb sublattice, e.g. ~ 20% (25%) of the Ge/Sb sites are vacant in $Ge_2Sb_2Te_5$ ($Ge_1Sb_2Te_4$). The structural disorder resulting from these vacancies is

expected to play an important role in controlling the thermodynamics and kinetics of transformation between *c*-GST and *a*-GST phases upon heating or laser irradiation. The inherent geometric instability of a lattice with such a large number of vacancies is borne out in the results reported in recent studies that the *c*-GST225 polymorph undergoes solid-state amorphization at high pressure and forms an amorphous phase, while the hexagonal GST225 polymorph remains crystalline and transforms into an orthorhombic phase at intermediate pressure and subsequently into a body-centered cubic (bcc) phase at high pressure [8,9]. Unfortunately, in spite of their key importance in the phase change phenomena, the atomic scale mechanisms and the thermodynamic phase stability relations of these complex structural transformations between the liquid, amorphous and various polymorphic crystalline GST phases are not well understood. Here we report the results of a synchrotron X-ray diffraction (XRD) study of the pressure and temperature dependent phase transformations in $Ge_1Sb_2Te_4$ at pressures of up to 44 GPa and temperatures of up to 838 K using a diamond anvil cell (DAC) to unravel these phase stability relations and their implications on phase change phenomena.

II. Experimental

For the synthesis of hexagonal $Ge_1Sb_2Te_4$ (*h*-GST124), stoichiometric mixtures of ≥99.995% purity (metals basis) elements were melted in evacuated (10^{-5} Torr), flame sealed fused silica ampoules at a temperature of 1073 K for at least 13 h in a rocking furnace and then quenched to room temperature, at which point they spontaneously crystallized into the desired hexagonal phase. In order to synthesize the *c*-GST124 phase, a 25mm target of *h*-GST124, prepared as above, was ablated onto a Teflon substrate with the focused beam (0.08cm^2 spot size) of a KrF excimer laser for 6 h. The resultant thin film was confirmed by XRD to consist of

cubic $Ge_1Sb_2Te_4$. The film was scraped off and used for subsequent diffraction measurements in a DAC.

X-ray diffraction and absorption data were collected on beamline 12.2.2 of the Advanced Light Source. A Si(111) double crystal monochromator was used for wavelength selection and diffraction data were collected using an energy of 25 keV (0.4959 Å) or 30 keV (0.4133 Å) and a sample to detector distance ranging between 230 and 300 mm. Absorption measurements were made using an energy of 30 keV. X-ray diffraction images were collected using either a mar345 image plate detector or a Bruker Platinum200 CCD detector. X-ray absorption was measured using a pindiode detector. Diffraction images were processed using the fit2d software package [10]. Sample densities were determined from a combination of diffraction and absorption data using the method of Shen et al. [11,12]. The Celref program [13] was used to determine unit cell parameters and volumes. High pressure measurements at ambient temperature were made using a standard symmetric DAC with 300μm culet diamonds and tungsten carbide and boron nitride backing plates on the synchrotron and detector sides, respectively. Rhenium gaskets were indented to a thickness of about 30μm. For diffraction measurements a 100μm hole was drilled in the center of the indentation and was loaded with sample, 4:1 methanol-ethanol mixture or liquid neon as the pressure transmitting fluid and small spheres of ruby and NaCl as pressure markers. For absorption measurements two 80μm holes were drilled in the indentation. One was filled with sodium chloride and the other with sample. High temperature measurements were made using a resistively heated DAC with a symmetric four pin design. Temperature was measured using a 'K' type thermocouple and was controlled to within ±1 K. Either gold or sodium chloride was used as a high temperature pressure marker, and liquid argon was used as a pressure transmitting fluid. Pressure was determined at high temperature using volumes of either

sodium chloride or gold determined from diffraction data together with the known equations of state [14,15].

Regarding the pressure calibration in these measurements, when ruby was used as a pressure marker the ruby fluorescence spectra showed a sharp doublet throughout our measurements with no measurable broadening of the peaks. A number of small ruby spheres were placed around the sample chamber. Pressure was measured from each of these spheres and differences in the measured pressure between these spheres were found to be within the experimental accuracy of the pressure scale used. The NaCl and Au pressure markers gave a number of sharp diffraction lines. All of these lines yielded unit cell parameters and hence volumes and corresponding applied pressures that were within the experimental accuracy expected from the synchrotron x-ray system used to measure the diffraction patterns. Diffraction data measured from our sample, with either Ne or methanol-ethanol mixture as the pressure transmitting fluid, were found to yield indistinguishable values as a function of pressure when plotted together. These results lead us to conclude that any non-hydrostaticity that might be present in our measurements was below a measurable level over the entire range of pressures and temperatures investigated in this study.

III. Results and Discussion

Room temperature XRD patterns of *c*-GST124 crystal collected under compression are shown in Fig. 1a. The compression cycle results in a simple shift of diffraction Bragg peaks to higher angles indicating a decrease in the unit cell dimensions. At pressures around 8.6 GPa, the intensities of the Bragg peaks for *c*-GST124 phase decrease and two broad bands appear at 14.1

GPa (Fig. 1a). Those broad bands can be attributed to gradual solid-state amorphization of *c*-GST124 above 14.1 GPa at room temperature. It may be noted here that in an alternative explanation one could consider that the broader peaks on which the sharper Bragg diffraction peaks are superimposed originate either from nanocrystals or from highly defective regions of the crystalline lattice. For example, upon increasing the pressure in a crystal with significant concentration of defects the latter can propagate and cluster [9]. Such nanometer-sized regions of highly defective crystals could also result in broad bands as those shown here, although it can be argued that structurally there could be no sharp demarcation between such highly defective crystals and an amorphous phase. The attribution of these broad diffraction bands to an amorphous phase is however, more sensible since the positions and widths of these broad bands agree remarkably well with those reported by Kolobov and coworkers in previous studies of pressure induced amorphization of the the *c*-GST225 polymorph where the amorphous bands were the dominant feature in the diffraction patterns [9]. Therefore, it is clear that the widths of the broad diffraction bands observed in this study are not related to the nanometric size of defective crystalline regions but instead they result from structural disorder of amorphous regions. Moreover, as discussed below, these amorphous patterns are characterized by a first sharp diffraction peak whose position is consistent with that observed in the corresponding melt phase when the effect of pressure is taken into account (*vide infra*).

The *c*-GST124 phase almost completely disappears at around 18.4 GPa and Bragg peaks for two new crystalline phases start to grow while some amorphous material remains up to 27.2 GPa in this experiment (Fig. 1a). The new crystalline phases can be indexed as orthorhombic with the space group *Pbnm (No.62)* and with unit cell dimensions *a*=2.91(1)Å, b=11.16(3)Å, *c*=3.59(1)Å and bcc (*Im-3m, No.229*) with unit cell dimension *a*=3.52(9)Å at 18.4 GPa and 24.5

GPa, respectively. The orthorhombic phase starts to transform into the bcc phase at higher pressures. Above 32.7 GPa the orthorhombic phase disappears and the bcc phase remains stable up to the highest pressure (44 GPa) (Fig. 1a). The ambient temperature bulk moduli of the *c*-GST124, orthorhombic and bcc phases, as obtained from fitting the pressure dependence of the unit cell volumes of these phases with a second-order Birch-Murnaghan equation of state, are 39.4, 45.2 and 54.4 GPa, respectively. These values, within experimental error bars of ±2 GPa, are similar to those reported in the literature for the corresponding GST225 phases [8,16].

In subsequent runs, *c*-GST124 was heated to a range of temperatures between 300 and 423 K at ambient pressure following which the pressure was increased (Figs. 1b, 1c). Similar to the room temperature behavior, the amorphous phase coexists with orthorhombic and bcc phases in the higher pressure regime. However, it is important to note that the onset pressure for solid-state amorphization shifts from 14.1 GPa at room temperature to lower pressures at higher temperatures (e.g., ~ 10 GPa at 423 K). Furthermore, in contrast with room temperature experiments, increase in pressure at higher temperatures results in a progressive drop in the relative concentration of the amorphous phase implying metastability of this phase and its thermally activated transformation to the high pressure orthorhombic and bcc phases (Figs. 1b, 1c). A comparison of the onset pressures at room temperature for amorphization of the *c*-GST124 phase as obtained in this study and of the *c*-GST225 phase as obtained in a previous study [8] indicates that the former structure with 25% vacancies in the Ge/Sb sites amorphizes at a significantly lower pressure (~ 14 GPa) compared to that (~ 22 GPa) for the latter structure with 20% vacancies. Therefore, pressure induced amorphization in GST phases is critically controlled by the presence and concentration of vacancies in the structure. Besides the structural effect of vacancies that presumably results in geometric instability and collapse at high pressure,

an increasing concentration of vacancies increases the configurational entropy of the crystal phase and brings it closer to the amorphous phase in terms of structural disorder. In this scenario solid-state amorphization will be kinetically favored i.e. *c*-GST phases with higher vacancy concentrations will display faster phase change kinetics. This happens to be indeed the case in GST alloys on the GeTe-Sb_2Te_3 tie line where compositions with higher Sb_2Te_3 concentration, i.e. with higher concentration of vacancies (e.g. *c*-GST124), show more rapid phase change compared to those with less Sb_2Te_3 (e.g. *c*-GST225) [17].

It is now well known that crystalline solids can be amorphized in the solid-state under compression at temperatures well below their usual melting point [18]. Usually such pressure-induced amorphization signifies the existence of a metastable amorphous phase which has a lower free energy compared to that of the parent crystal but the transformation into a more stable high-pressure crystalline phase is kinetically hindered. It is clear from Fig. 1 that the amorphized *c*-GST124 phase is indeed metastable and undergoes thermally activated conversion into the orthorhombic and bcc phases with increasing pressure. It is tempting to speculate that the pressure induced solid-state amorphization of the *c*-GST124 phase in the metastable region at low temperature range might lead to changes in bonding and electronic structure that are similar to those that accompany the fcc to orthorhombic transition in the stable region (Fig. 1). The latter transition has been investigated in detail for GeTe in previous studies [19]. The results of these studies have indicated that the distorted rocksalt structure of GeTe is stabilized by the octahedral resonance bonding with three p orbitals associated with the valence band while, upon compression, shortening of interatomic distances results in s-p hybridization and covalent bonding. Such metallic to covalent transition during the crystalline to amorphous phase change in GST materials can indeed explain the large differences in optical and electronic properties

between the two phases that are central to their application in optical and electronic memory devices [20].

As mentioned above, the onset pressure for solid-state amorphization of the *c*-GST124 phase decreases with increasing temperature implying a negative Clapeyron slope for the transition. The Clapeyron slope $dP/dT = \Delta S/\Delta V$ where ΔS and ΔV denote changes in entropy and molar volume, respectively, across a phase transition. Since the entropy of *a*-GST124 is expected to be higher than that of c-GST124, ΔS for amorphization is positive. Therefore, a negative Clapeyron slope implies that *a*-GST124 is denser than *c*-GST124. This expectation is consistent with the results of an *ab initio* molecular dynamics simulation of the amorphization of *c*-GST225 phase reported in a previous study, where the density of the *a*-GST phase was found to be higher than the *c*-GST phase at high pressures [21]. The higher density of the *a*-GST124 phase is also consistent with its significantly higher compressibility (bulk modulus B ~ 18 GPa) as reported in a previous study [22] compared to that of *c*-GST124 (B ~ 39 GPa).

The *c*-GST124 phase was found to convert to the hexagonal polymorph *h*-GST124 at temperatures higher than 423 K for experiments at pressures below ~ 7 GPa, consistent with previous results obtained at ambient pressure [5]. At intermediate temperatures between 550 and 650 K, upon increasing pressure the hexagonal phase often coexists with the orthorhombic phase and finally completely converts to the orthorhombic phase at higher pressures (Fig. 2a). This result is consistent with the fact that, for ambient temperature experiments that used *h*-GST124 as the starting material, this phase was found to undergo a transition into the orthorhombic phase upon compression at ~ 12 GPa and finally into the bcc phase at ~ 30 GPa (Fig. 2b).

Most interestingly, the melting temperature of the hexagonal phase at pressures ranging between ambient and ~ 7 GPa decreased with increasing pressure i.e. the melting of *h*-GST124 is

characterized by a negative P-T slope. Typically during melting both the entropy and volume of the resulting liquid are expected to be higher than those of the crystal i.e. both ΔS and ΔV are positive and hence the Clapeyron slope for melting is also expected to be positive. However, the existence of a high density liquid phase incorporating more closely packed atomic configurations than those occurring in the crystal would mean that ΔV could be negative and, with ΔS positive, the Clapeyron slope of the melting curve would be negative. It is to be noted that a negative P-T slope for melting has also been experimentally observed in the case of Sb_2Te_3 at pressures below 5 GPa [23].

The pressure and temperature dependent phase stability relations for GST124 as obtained from the experiments carried out in this study are comprehensively summarized in Fig. 3. The P-T phase boundary for melting of *h*-GST124 yields a slope $dP/dT = 0.025$ GPa.K^{-1} while the P-T line of solid state amorphization of the *c*-GST124 that corresponds to the first appearance of the amorphous phase is characterized by $dP/dT = 0.033$ GPa.K^{-1}. These two lines follow each other quite closely upon linear extrapolation to low (high) temperatures and high (low) pressures (Fig. 3). It may be noted that unlike melting, amorphization is not a first order thermodynamic transition and is strongly kinetically controlled, presumably via nucleation and growth. Therefore, P-T line denoting the first appearance of the amorphous phase is not a true thermodynamic phase boundary. However, when taken together, the similarities in the dP/dT slope and in the location in P-T space of the lines corresponding to the melting transition of *h*-GST124 and to the solid state amorphization of the *c*-GST124 strongly suggest that the metastable amorphous phase most likely corresponds to the high pressure thermodynamic melting of the parent *c*-GST124 phase at a significantly lower temperature due to the negative Clapeyron slope for the melting transition. In practice this thermodynamic melting of *c*-GST124

is not observed as at high pressure the phase stability field of *c*-GST124 and its melt is truncated by the appearance of the orthorhombic and bcc phases as discussed above. The P-T line for high pressure melting of the *c*-GST124 phase would be expected to be somewhat vertically shifted to higher temperatures with respect to the solid state amorphization line as the latter would be closer to the glass transition temperature of this high pressure melt. This hypothesis is consistent with the fact that the extrapolated P-T phase boundary of the melting transition of *h*-GST124 is situated at higher temperatures with respect to the P-T line for solid state amorphization (Fig. 3). Additional support for this hypothesis comes from the fact that the linear pressure dependence of the position of the first sharp diffraction peak (FSDP) of the GST124 liquid, supercooled liquid and glassy phases, when extrapolated to high pressures, corresponds remarkably well with the position of the FSDP of the solid state amorphized phase within experimental error (Fig. 4). Such a linear dependence of the position of the FSDP on pressure is not surprising since both variables are expected to scale linearly with molar volume and has indeed been experimentally observed in previous studies [24,25]. Therefore, the results shown in Fig. 4 indicate that the GST124 liquid, glass and solid state amorphized phases have similar pressure dependence of molar volume i.e. similar bulk moduli.

Direct x-ray absorption based measurements of the densities of the *h*-GST124 and the melt phases were carried out at 3.75 GPa across the melting point near 780 K. Such measurements yield densities of 7.1±0.3 and 7.6±0.3 $g.cm^{-3}$, respectively, for the crystal and the melt phases. Similar measurements for the *c*-GST124 and the *a*-GST124 phases were carried out at ambient temperature across the amorphization pressure of 14 GPa and densities of 6.9±0.3 and 7.1±0.3 $g.cm^{-3}$ were obtained for the crystalline and amorphous phases, respectively. These results demonstrate that ΔV is indeed negative for both melting and amorphization transitions,

consistent with the observation of negative Clapeyron slopes for both transitions (Fig. 3). Approximating the bulk modulus of the GST124 melt to be independent of temperature and similar to that of *a*-GST124 yields a density of 6.3±0.2 g.cm^{-3} for the melt at ambient pressure at 780 K. This density is ~ 4.5% lower than that of the *c*-GST124 phase (~ 6.6±0.2 g.cm^{-3}) at ambient conditions. Therefore, melting of a confined crystalline bit during optical phase change recording will generate a maximum internal pressure of ~ 1 GPa due to net expansion associated with melting if thermal expansion of the melt between 780 K and the melting point of 888 K at ambient pressure is neglected. This pressure value is low enough such that the pressure-temperature-time path traversed by the system during melting and recrystallization will be largely enclosed within the stability field of the crystalline GST phases (Fig. 3). Therefore, such internal pressures would not play an important role in stabilizing the amorphous phase upon quenching of the molten bit as had been claimed in previous studies [8]. However, these pressures generated during melting and recrystallization of bits in phase change random access memory (PRAM) structures are high enough to affect the long-term reliability against mechanical failure of the device [26,27].

IV. Summary

The pressure and temperature induced phase transformations of the GST124 phase change alloy have been investigated using high-resolution x-ray diffraction over a wide range of P-T conditions. The crystalline *c*-GST124 phase begins to undergo solid state amorphization at pressures ranging between 10 and 14 GPa at relatively low temperatures between ambient and 423 K. The onset pressure for solid state amorphization of *c*-GST124 decreases with increasing temperature implying a negative Clapeyron slope for this phase transformation. The amorphous

phase is metastable and it undergoes thermally activated transformation into orthorhombic and bcc phases with increasing pressure. The bcc phase is found to be the most stable polymorph at the highest pressures. A comparison with the previously published results on the *c*-GST225 phase indicates that increasing vacancy concentration in the *c*-GST phase kinetically facilitates the pressure induced solid state amorphization process. It is likely that this amorphization of the *c*-GST124 results in changes in bonding and electronic structure corresponding to a metallic-to-covalent transformation that may be responsible for the large difference in the optical and electronic properties associated with the phase change process utilized in memory devices.

The *c*-GST124 converts to the *h*-GST124 phase at temperatures higher than 423 K for pressures below ~ 7 GPa. Melting of the *h*-GST124 at higher temperatures display a negative Clapeyron slope implying the formation of a liquid phase that is denser than the parent crystal. When taken together, the Clapeyron slopes and the location of the phase boundaries in the P-T space for the solid state amorphization of *c*-GST124 and the melting of *h*-GST124 indicate that the former transformation may be a metastable extension of the latter, at lower temperatures and higher pressures. Finally, the magnitudes of the internal pressures generated during phase change are estimated and found to be significant for thermomechanical stress development and related reliability issues in PRAM devices.

Acknowledgments:

The authors thank S.C. Currie for synthesis of *h*- and *c*-GST124. S.S. was supported by NSF-DMR grant 0907060. The Advanced Light Source is supported by the Director, Office of Science, Office of Basic Energy Sciences, of the U.S. Department of Energy under Contract No. DE-AC02-05CH11231.

References:

1. M. Wuttig and N. Yamada, Nature Mater. **6**, 824 (2007), and references therein.
2. M. Wuttig, Nature Mater. **4**, 265 (2005).
3. E.R. Meinders, A.V. Mijritskii, L. van Pieterson and M. Wuttig, *Optical Data Storage: Phase Change Media and Recording* (Springer, Berlin, 2006).
4. T. Matsunaga and N. Yamada, Phys. Rev. B **69**, 104111 (2004).
5. N. Yamada, E. Ohno, K. Nishiuchi, N. Akahira and M. Takao, J. Appl. Phys. **69**, 2849 (1991).
6. J. Kalb, F. Spaepen, M. Wuttig, J. Appl. Phys. **93**, 2389 (2003).
7. J. A. Kalb, M. Wuttig, F. Spaepen, J. Mater. Res. **22**, 748 (2007).
8. A. V. Kolobov, J. Haines, A. Pradel, M. Ribes, P. Fons, J. Tominaga, Y. Katayama, T. Hammouda, T. Uruga, Phys. Rev. Lett. **9**7, 035701 (2006).
9. M. Krbal, A. V. Kolobov, J. Haines, P. Fons, C. Levelut, R. Le Parc, M. Hanfland, J. Tominaga, A. Pradel, M. Ribes, Phys. Rev. Lett. **103**, 115502 (2009).
10. A.P. Hammersley, S.O. Svensson, M. Hanfland, A.N. Fitch, D. Hausermann, High Pressure Research **14,** 235 (1996).
11. G. Shen, N. Sata, N. Taberlet, M. Newville, M.L. Rivers and S.R. Sutton, J. Phys. Cond. Matt. **14**, 10533 (2002).
12. X. Hong, G. Shen, V.B. Prakapenka, M.L. Rivers and S.R. Sutton, Rev. Sci. Inst. **78**, 103905 (2007).

13. J. Laugier, B. Bochu, CELREF. Version 3. Cell parameter refinement program from powder diffraction diagram, Laboratoire des Matériaux et du Génie Physique, Ecole Nationale Supérieure de Physique de Grenoble (INPG), France (2002).

14. F. Birch, J. Geophys. Res. **91**(B5), 4949 (1986).

15. D. Heinz, R. Jeanloz, J. Appl. Phys. **55**, 885 (1984).

16. M. Krbal *et al.*, Appl. Phys. Lett. **93**, 031918 (2008).

17. J. Akola, R. O. Jones, Phys. Rev. B **79**, 134118 (2009).

18. S.M. Sharma, S.K. Sikka, Prog. Mater. Sci. **40**, 1 (1996).

19. T. Suski, J . Karpinski, K.L. I. Kobayashi, K. F. Komatsuba, J. Phys. Chem. Solids **42**, 479 (1981).

20. A.V. Kolobov, P. Fons, A.I. Frenkel, A.L. Ankudinov, J. Tominaga, T. Uruga, Nature Mater. **3**, 703 (2004).

21. S. Caravati, M. Bernasconi, T.D. Kuhne, M. Krack, M. Parinello, Phys. Rev. Lett. **102**, 205502 (2009).

22. T. Blachowicz *et al.,* J. Appl. Phys. **102**, 093519 (2007).

23. L.G. Khvorostyantsev *et al.*, Phys. Status Solidi **A89**, 301 (1985).

24. Y. Inamura, Y. Katayama, W. Utsumi, K. Funakoshi, Phys. Rev. Lett. **93**, 015501 (2004).

25. S.R. Elliott, Phys. Rev. Lett. **67,** 711 (1991).

26. T.P. Leervad Pedersen, J. Kalb, W.K. Njoroge, D. Wamwangi, M. Wuttig, Appl. Phys. Lett. **79**, 3597 (2001).

27. K.N. Chen, C. Cabral Jr., L. Krusin-Elbaum, Microelectronic Engineering **85**, 2346 (2008).

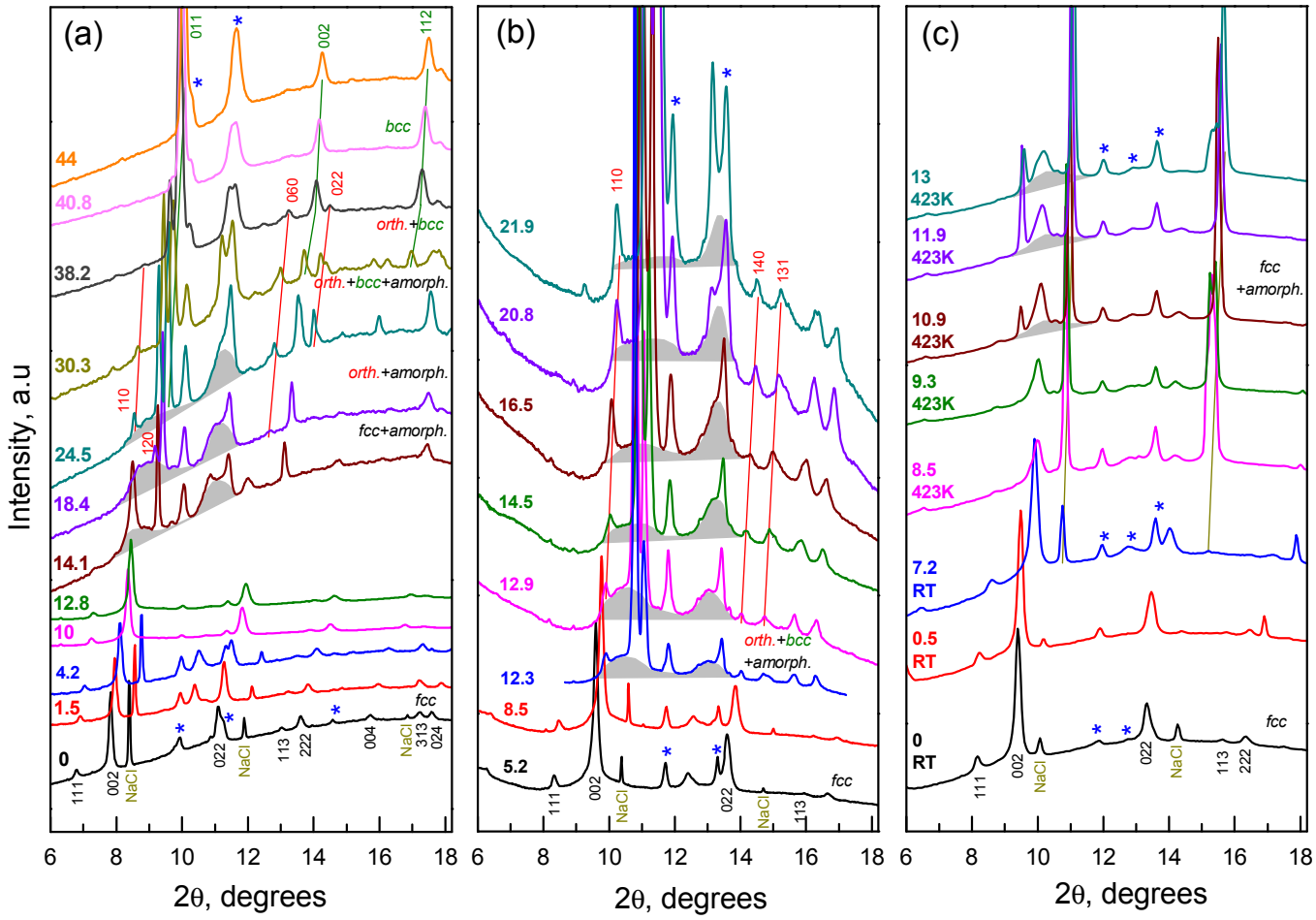

Fig. 1 (color)**.** XRD patterns collected at (a) 298 K, (b) 373 K and (c) 423 K during compression of *c*-GST124. Miller indices indicate the observed reflections of cubic (black), orthorhombic (red) and bcc (green) phases of GST124; NaCl (dark yellow) pressure marker; Rhenium (blue asterisks) gasket material. Solid lines follow the peak positions of relevant phases. Corresponding pressures in GPa are given to the left of each pattern. Grey shaded bands represent diffraction peaks from the amorphous phase. Operating X-ray wavelengths are 0.4133, 0.4859 and 0.4959 Å, respectively, for (a), (b) and (c).

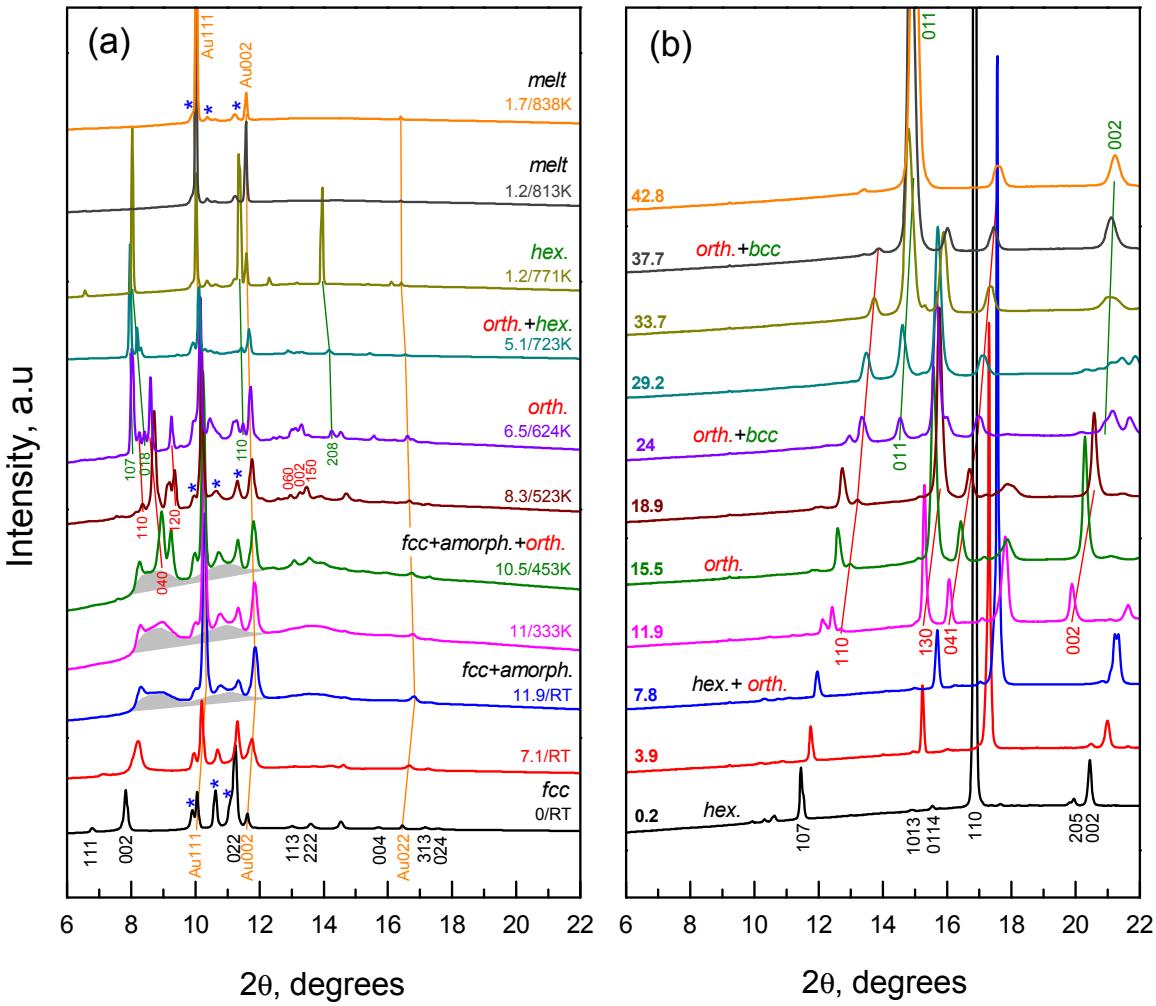

Fig. 2 (color)**.** (a) In-situ XRD patterns collected during compression and heating of *c*-GST124 in the pressure range of 0-12 GPa and temperatures up to 838 K (indicated alongside each pattern). Grey shaded bands represent diffraction peaks from the amorphous phase. (b) XRD patterns of *h*-GST124 collected at 298 K upon compression. Miller indices indicate the observed reflections of cubic (black), orthorhombic (red), bcc and hexagonal (green) phases of GST124; Au (orange) pressure markers; Rhenium (blue asterisks) gasket material. Solid lines follow the peak positions of relevant phases. Operating X-ray wavelengths are 0.4133 and 0.6199 Å, respectively, for (a) and (b).

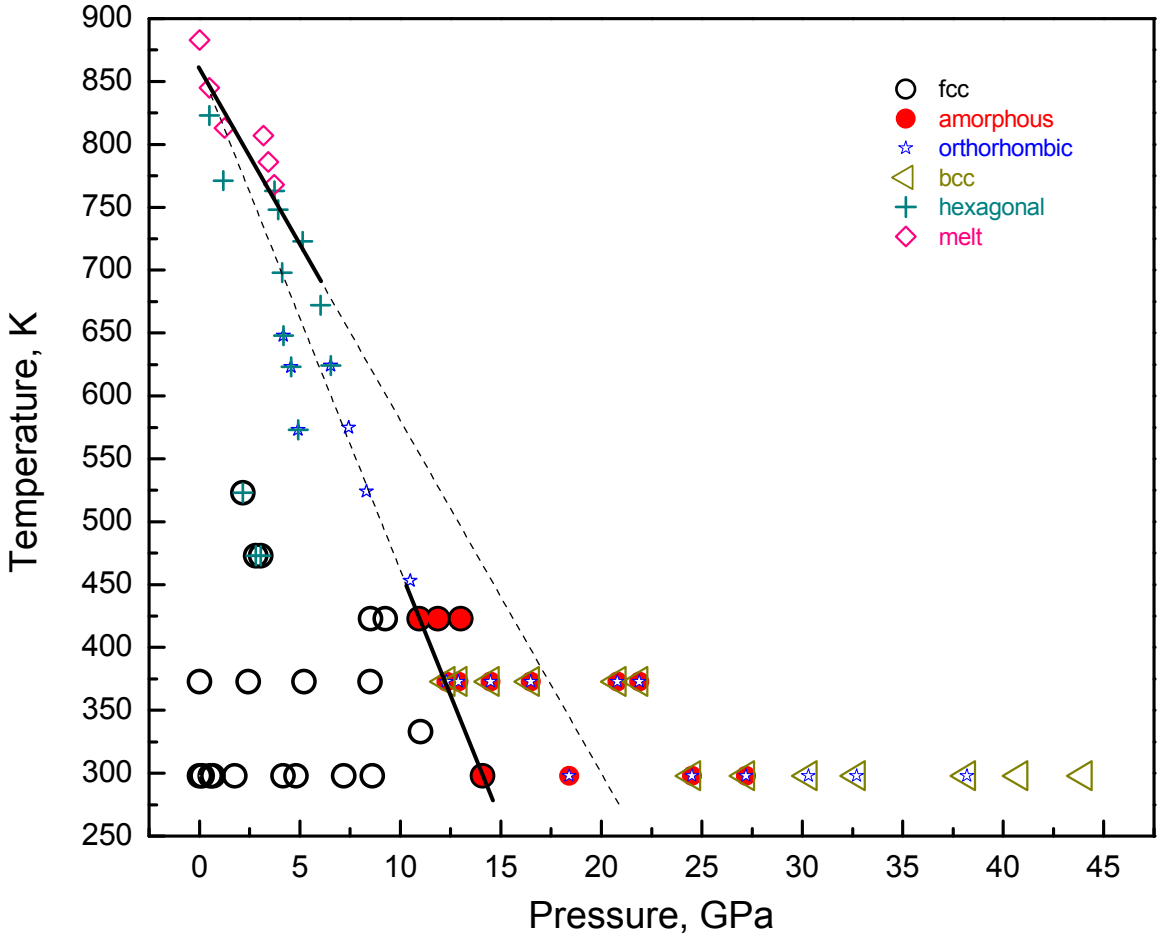

Fig. 3 (color). Phase diagram of GST124 in the studied temperature and pressure range as determined by in-situ XRD experiments. Phase relations are established using data presented in this work. The symbols represent the relevant phases. The solid black lines denote phase boundaries corresponding to *hexagonal-to-melting* and *fcc-to-amorphous* transitions. The phase boundary for the latter transition corresponds to the first appearance of the amorphous phase. Dashed lines are the corresponding linear extrapolations.

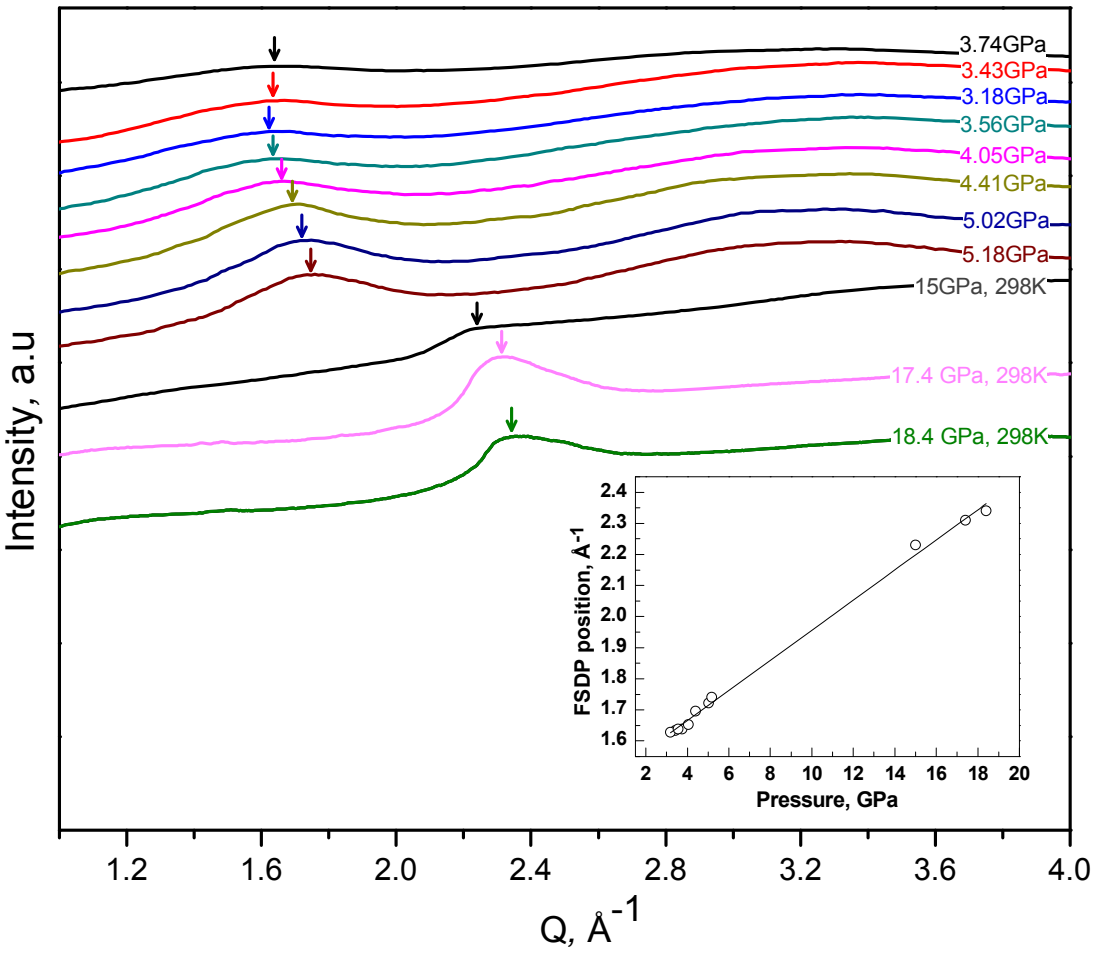

Fig. 4 (color). X-ray scattering from GST124 melt, supercooled liquid and glassy phases collected upon quenching from 807 K to 307 K in the 3.1-5.1 GPa pressure range as a function of scattering wavevector Q (after subtraction of the diffraction peaks due to the gasket and the internal P-T calibrants). The bottommost curve at 15 GPa is the pressure-amorphized phase of *c*-GST124 presented on the same scale. Arrows follow the position of the first sharp diffraction peak (FSDP). The inset presents the pressure dependence of FSDP position. Solid black line shows the linear least squares fit through all data points.